Interplay of 4f and 3d moments in $EuFe_2As_2$ iron pnictides

Jannis Maiwald and Philipp Gegenwart*

Experimentalphysik VI, Universität Augsburg, Universitätsstraße 1, 86135 Augsburg, Germany

* Corresponding author: e-mail philipp.gegenwart@physik.uni-augsburg.de, Phone: +49-821-5983650, Fax: 49-821-5983652

$EuFe_2As_2$ is unique among 122 iron pnictides due to its 4f magnetic moments. We review its properties with particular emphasis on the interplay between 4f and 3d moments. After discussing the parent compound, we first focus on the evolution of magnetism and superconductivity for hole-doped $Eu_{1-x}K_xFe_2As_2$ as well as for chemical and hydrostatic pressure in $EuFe_2(As_{1-x}P_x)_2$. Non-Fermi liquid behavior for optimally doped superconducting systems is highlighted in the electrical resistivity and thermoelectric power. We also discuss the in-plane anisotropy and how the indirect magnetoelastic coupling between Eu 4f moments and the crystal structure can be used for persistent detwinning of $EuFe_2As_2$ in the orthorhombic state by small magnetic fields.

1 Introduction Since the discovery by Hosono's group [1], tremendous work has been performed on Fe-based superconductors [2–6]. Materials in a variety of different crystal structures have been investigated, which commonly exhibit iron-pnictide or iron-chalcogenide layers, being responsible for superconductivity (SC). For understanding the fundamental properties of these superconductors, the so-called "122" systems AFe_2As_2 (A = Ca, Sr, Ba, Eu), crystallizing in the tetragonal $ThCr_2Si_2$ structure, are well suited [7]: these systems could be grown as large and clean single crystals by flux techniques and there are various ways to tune the electronic properties. For example, SC is induced by substitutions on either one of the three lattice sites as well as by hydrostatic pressure. There are many possibilities for hole- and electron doping. Isovalent substitution could be used to induce chemical pressure.

AFe_2As_2 systems undergo a structural distortion from tetragonal to orthorhombic upon cooling from room temperature through T_s and subsequent antiferromagnetic (AF) ordering at T_N due to the formation of a spin-density-wave (SDW). SC appears as these transitions are suppressed by doping or pressure. Analogous behavior is found in other unconventional superconductors like cuprates, organics, or heavy-fermions, where different electronically ordered states such as Mott insulators, pseudogap, magnetic order, or electronic nematic phases are in competition with SC. Often the maximal transition temperature $T_{c,max}$ is found at such doping or pressure where the suppressed competing order leads to a quantum phase transition. In addition, there is growing evidence for non-Fermi liquid (NFL) normal state behavior at $T > T_{c,max}$, which could be related to quantum criticality. It is of particular interest, with respect to iron pnictides, to investigate the nature of the electronic order competing with SC, its anisotropic fluctuations [8], the relation to quantum criticality, as well as consequences for the SC order parameter.

In this review, we focus on $EuFe_2As_2$-based iron pnictide systems. In contrast to AFe_2As_2 with nonmagnetic A = Ca, Ba, or Sr, Eu-based materials are special due to their local 4f magnetic moments, which order antiferromagnetically around 19 K. However, a metamagnetic transition to a ferromagnetic state can be induced by application of small, in-plane magnetic fields of the order of 1 T [9–11]. We review the intricate interplay of these Eu^{2+} moments with SC, magnetic and structural order related to 3d electrons. The paper is organized as follows: first, we discuss the structural and magnetic properties of the $EuFe_2As_2$ parent compound and then examine the effect of hole- and isovalent-doping together with the application of external pressure on those properties. We also focus on non-Fermi liquid behavior in the electrical resistivity and the thermoelectric power (TEP) in both doping series. Finally, we assess in detail the effect of external magnetic fields on the distribution of structural twin domains, which form in the low-temperature orthorhombic phase.

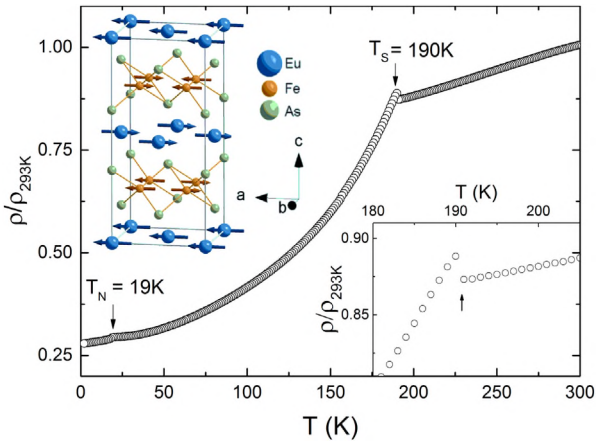

Figure 1 Temperature dependence of the in-plane electrical resistivity of $EuFe_2As_2$. The two arrows indicate the structural and 3d magnetic ordering at $T_s \approx 190$ K and 4f AF ordering at $T_N = 19$ K, respectively. The inset shows an enlarged view in the region near T_s. The magnetic ground state is sketched in the top left inset (replotted from Ref. [10]).

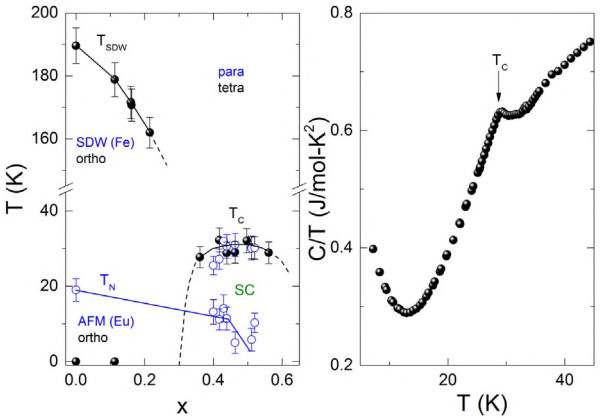

Figure 2 (Left) Phase diagram of $Eu_{1-x}K_xFe_2As_2$ [17]. Filled (black) circles illustrate phase transition temperatures extracted from resistivity measurements, while open (blue) circles indicate transition temperatures derived from susceptibility data. Solid and dashed lines are guides to the eye. (Right) Specific heat over temperature C/T as a function of temperature for a sample with composition $x = 0.5$ [20]. The arrow indicates the superconducting transition.

2 Magnetic order in $EuFe_2As_2$ Like other compounds of the 122 family of the iron pnictides, $EuFe_2As_2$ crystallizes in the $ThCr_2Si_2$ crystal structure with space group I4/mmm. Layers of $[FeAs]^{2-}$ are stacked with spacer layers of Eu^{2+}. At high temperatures, the system is in a paramagnetic state with a tetragonal crystal structure ($a = 3.908(3)$ Å, $c = 12.165(7)$ Å) [12, 13]. At $T_s \approx 190$ K, the system exhibits a combined transition of structural and SDW ordering of Fe 3d moments. More precisely, an orthorhombic lattice distortion into space group Cmma and a columnar AF arrangement of Fe moments is found [10], as indicated by the orange-colored arrows in the inset of Fig. 1. Distinct from other 122 pnictides, $EuFe_2As_2$ contains 4f Eu^{2+} magnetic moments. They order in an A-type AF structure below $T_N = 19$ K, as sketched by blue arrows in the inset of Fig. 1. This ordering consists of ferromagnetic (FM) layers of 4f moments aligned along the crystallographic a-axis, which are stacked antiferromagnetically along the c-axis [10].

As displayed in Fig. 1 the electrical resistivity $\rho(T)$, measured within the tetragonal plane decreases slightly upon cooling from room temperature down to T_s, where it displays a sharp increase, attributed to the SDW gap formation [12]. Another change in slope is found at T_N due to the 4f magnetic ordering. Typical values for the in-plane electrical resistivity are $\rho(300\,\mathrm{K}) = 630\,\mu\Omega$cm and $\rho(2\,\mathrm{K}) = 200\,\mu\Omega$cm at high and low temperatures, respectively. The resistivity along the c-axis is about eight times larger than the in-plane resistivity but follows a similar temperature dependence [14].

Band-structure calculations indicate that the electronic structure of $EuFe_2As_2$ is overall similar to its sister $SrFe_2As_2$ with no 4f moments [12]. Accordingly, $EuFe_2As_2$ can be tuned into a high-T_c superconducting state by similar means as Ba-, Sr-, and Ca-122 compounds. In particular, chemical doping with electrons or holes, as well as chemical or hydrostatic pressure induces SC [15–19].

3 Hole doping According to angle-resolved photo emission spectroscopy (ARPES) data, the unreconstructed, quasi two-dimensional (2D) Fermi surface of $EuFe_2As_2$ consists of three hole-like sheets at the Brillouin zone center near the Γ-point ($\mathbf{k} = (0, 0)$) and two electron-like sheets at the corners near the M-point ($\mathbf{k} = (\pi, \pi)$) [21, 22]. Time-resolved ARPES has revealed ultrafast single- and many-particle dynamics in $EuFe_2As_2$ and the momentum averaged electron-phonon coupling has been quantified [23, 24]. The outer hole sheet has a more 3D character compared to the two other more 2D hole sheets, due to a larger dispersion along $\mathbf{k}_z$. The SDW ordering can be related to Fermi surface nesting. The corresponding nesting vector $\mathbf{Q}_n$ lies along the Γ–M direction. Partial substitution of Eu^{2+} by K^{1+} atoms expands the hole Fermi surface sheets, while the electron sheets in the k_xk_y-plane shrink. This causes a weakening of the nesting condition, which in turn leads to a suppression of the SDW ordering temperature [22].

The phase diagram for $Eu_{1-x}K_xFe_2As_2$ is shown in the left part of Fig. 2. Upon K-doping up to $x = 0.2$ in $Eu_{1-x}K_xFe_2As_2$ T_s continuously reduces to approximately 160 K. Beyond this composition, the SDW order rapidly disappears. Above $x > 0.3$ SC sets in, reaching a maximal $T_c \approx 34$ K at the optimal doping of about $x_{max} = 0.5$ [16, 17]. The bulk nature of the SC has been confirmed by a clear jump in the specific heat [20] (Fig. 2) and a strong Meissner effect in the magnetic susceptibility [16]. Optical conductivity has revealed a gap $2\Delta_0 = 9.5\,\mathrm{meV} = 3.7\,k_BT_c$ with s-wave symmetry and no nodes [25]. The electron spin resonance of Eu^{2+} spins displays no Hebel–Slichter peak below T_c and the spin-lattice relaxation rate follows $1/T_1^{ESR} \sim T^{1.5}$ [26]. The upper critical field H_{c2} amounts to 55 and 65 T for fields parallel and perpendicular to the c-axis, respectively [27].

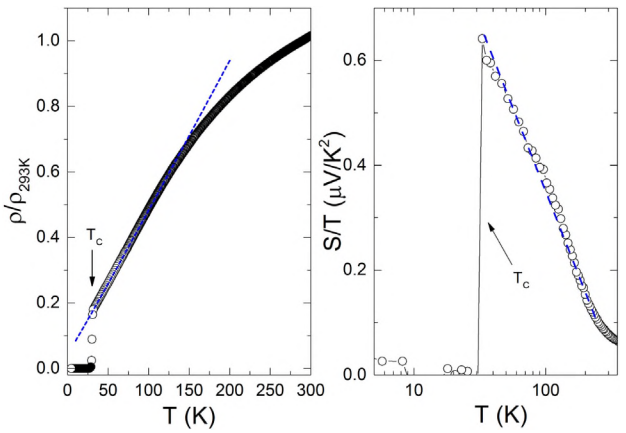

Figure 3 (Left) Normalized in-plane electrical resistivity of a near optimally doped ($x = 0.51$) $Eu_{1-x}K_xFe_2As_2$ single crystal. The dashed line indicates the non-Fermi liquid temperature dependence $\rho(T) = \rho_0 + AT^n$ with exponent $n = 1.03$. (Right) Seebeck coefficient divided by temperature S/T versus log T. The slightly underdoped ($x = 0.44$) crystal exhibits strong signs of a logarithmic divergence of S/T, compatible with a magnetic quantum critical point in the phase diagram. The dashed line is a guide to the eye. Data taken from Ref. [17].

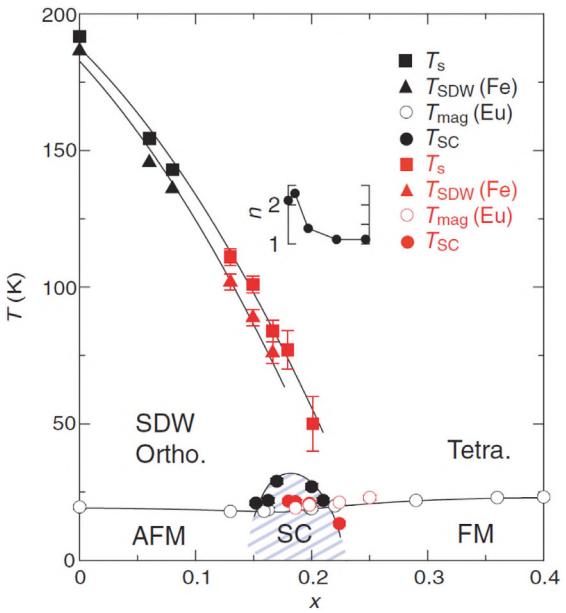

Figure 4 Phase diagram of $EuFe_2(As_{1-x}P_x)_2$ as derived from single crystals at ambient (black symbols) and hydrostatic pressure (red symbols) [32].

The dilution of the Eu^{2+} magnetic sublattice leads to a weakening of 4f magnetic ordering and eventual change from a long-range ordered into a glassy frozen (i.e., short-ranged) state near $x = 0.5$. The temperature dependence of the magnetic penetration depth reveals a dip near 5 K related to short-ranged ordering of 4f moments [28]. Due to problems in crystal growth, there have been no systematic investigations in the doping regime between $x = 0.55$ and $x = 1$. The end member KFe_2As_2 displays a significantly lower SC transition temperature of $T_c = 3.4$ K [29].

The suppression to the SDW order as well as the emergence of SC would be compatible with a quantum critical point (QCP) in the phase diagram of $Eu_{1-x}K_xFe_2As_2$. In order to search for signatures of quantum criticality, we have carefully investigated the temperature dependencies of the electrical resistivity and TEP for near optimally doped $Eu_{1-x}K_xFe_2As_2$ above the superconducting transition, cf., Fig. 3. Indeed the electrical resistivity $\rho(T)$ follows a linear temperature dependence between T_c and 150 K while the TEP coefficient S/T displays an almost logarithmic divergence in the same temperature regime [17]. Similar behavior has also been found in K-doped $SrFe_2As_2$ [30]. These temperature dependencies would agree with the prediction for a 2D SDW QCP [31]. However, the temperature range above T_c is too small in order to draw solid conclusions about quantum criticality. The hole-doping dependence of the TEP $S(x)_{T=\text{const}}$ in $Eu_{1-x}K_xFe_2As_2$ has revealed clear anomalies near $x = 0.3$, which suggest a Lifshitz transition, related to the suppression of the SDW ordering [17].

4 Chemical and hydrostatic pressure Early hydrostatic pressure experiments on $EuFe_2As_2$ have revealed the suppression of SDW ordering and onset of SC for pressures beyond 2.5 GPa [18, 19]. Since isovalent substitution of As by the smaller P in $EuFe_2(As_{1-x}P_x)_2$ leads to a linear decrease of the c-lattice parameter and unit cell volume with x [33], hydrostatic and chemical pressure should result in similar effects on the physical properties of $EuFe_2As_2$. Indeed pressure experiments on selected $EuFe_2(As_{1-x}P_x)_2$ single crystals, revealed a one-to-one correspondence between the P content and the applied hydrostatic pressure. The obtained phase diagram of $EuFe_2(As_{1-x}P_x)_2$ is shown in Fig. 4 [32]. Most importantly, SC is confined to a very narrow range between $x = 0.18$ and 0.23. In contrast to other 122 pnictides, SC in $EuFe_2(As_{1-x}P_x)_2$ does not form over a broad range of the phase diagram like, e.g., in $BaFe_2(As_{1-x}P_x)_2$ [34, 35], extending beyond the suppression of the SDW ordering. This could either be related to the ordering of Eu 4f moments, which may act detrimental on SC despite the occurrence of SC and FM Eu ordering in a $x = 0.3$ polycrystal [36, 37], or more likely, due to the electronic changes induced by a Lifshitz transition of the inner hole-Fermi surface (see below). Another difference in the phase diagram to other 122-type iron pnictides is not only the presence of the low-temperature AF phase stemming from 4f-moments of Eu, but a phase transition of these moments to a FM configuration with increased P-doping.

ARPES measurements on $EuFe_2(As_{1-x}P_x)_2$ indicate that chemical pressure leaves the electron Fermi surface sheets basically unchanged, while the hole sheets develop a more 3D character due to the c-axis compression and decreasing c/a ratio [33]. This leads to a continuous suppression of the SDW ordering and structural phase transition, as indicated in the phase diagram in Fig. 4.

In contrast to the case of $Eu_{1-x}K_xFe_2As_2$, where the Eu site is diluted and thus long-range ordering of 4f moments becomes weakened and suppressed, the Eu sublattice remains intact for $EuFe_2(As_{1-x}P_x)_2$. From magnetization measurements for magnetic fields within the ab-plane, it has been deduced, that the 4f ordering changes its character from AF to FM at P concentrations beyond $x = 0.23$ [33]. Recent neutron scattering has shown that the Eu 4f moments order ferromagnetically along the c-axis already for $x = 0.19$ [38]. The proposed canted AF order, deduced from bulk magnetization measurements [39] could not be confirmed [38]. As shown in the phase diagram displayed in Fig. 4, after a sufficient suppression of the iron ordering, SC emerges in the system with a maximal transition temperature of $T_c^{max} = 28$ K around $x = 0.19$. In a narrow region SC coexist with the Eu^{2+} order [33], while the system is likely still in an orthorhombic SDW state [33, 32]. In-plane magnetization has suggested that at a slightly higher doping level of $x \approx 0.23$, the Eu^{2+} order changes abruptly to FM and SC disappears [39]. Several effects appear to happen simultaneously around this critical concentration: our TEP data show a distinct, non-monotonic evolution of $S(x)$ at constant temperature, indicating a Lifshitz transition [17]. Further evidence for such a transition was found by Thirupathaiah et al. Their ARPES measurements indicate the vanishing of the inner hole-Fermi surface sheet at this concentration [40]. At $x > 0.2$, the electronic and structural phase transitions are likely fully suppressed [32].

Fermi surface nesting can have a strong influence on the Ruderman–Kittel–Kasuya–Yosida (RKKY) interaction in multiband systems by modifying its strength and anisotropy [41]. The evolution of the indirect exchange coupling likely causes the rearrangement of the magnetic order of the Eu^{2+} moments beyond the critical concentration. Furthermore, LDA+U calculations suggest that the Eu ordering in the parent compound is close to an instability toward ferromagnetism [33]. Clearly, the narrowness of the SC dome in $EuFe_2(As_{1-x}P_x)_2$ is not caused by disorder, as it has been confirmed by hydrostatic pressure experiments [32].

Previously, the following scenario has been proposed to account for the phase diagram of $EuFe_2(As_{1-x}P_x)_2$ [32]: A Lifshitz transition around $x = 0.23$ breaks the Fermi surface nesting and hence suppresses the SDW transition which in turn impedes the structural transition. The disappearance of the SDW transition changes the RKKY interaction and – in agreement with the LDA+U calculations – increases interlayer coupling which leads to a FM arrangement of the Eu^{2+} moments. The FM state may be incompatible with the s^{+-}-wave paring proposed for this system [4, 33, 42], because the Zeeman effect, which arises due to the FM order, strongly disfavors the formation of Cooper pair singlets. However, recent resonant magnetic x-ray scattering as well as neutron scattering have confirmed the microscopic coexistence of SC with FM Eu ordering in which moments of $6.6\mu_B$ are primarily aligned along the c-axis [38, 43]. Furthermore, hydrostatic pressure experiments at 3.2 GPa on $EuFe_2As_2$ reveal a broader SC dome, extending beyond the vanishing of the structural and SDW order [44].

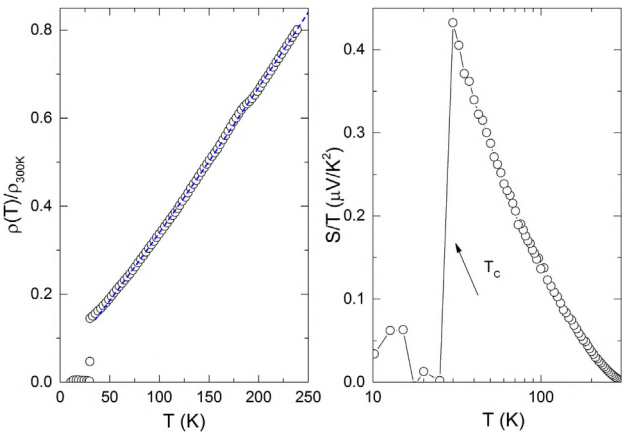

Figure 5 (Left) Normalized electrical resistivity of an almost optimally doped ($x = 0.20$) $EuFe_2(As_{1-x}P_x)_2$ single crystal. The dashed line indicates the non-Fermi liquid temperature dependence with $\rho(T) = \rho_0 + AT^n$ with $n = 1.09$. Data extracted from Ref. [33]. (Right) Seebeck coefficient divided by temperature S/T vs $\log T$. The optimally doped ($x = 0.21$) crystal exhibits strong signs of a logarithmic divergence of S/T, suggesting a magnetic quantum critical point in the phase diagram. Data replotted from Ref. [17].

In the context of 4f magnetic ordering we finally mention, that a careful study of the magnetization and differential susceptibility at very small magnetic fields below 0.1 T has revealed indications for a "re-entrant spin-glass" freezing at temperatures below the magnetic ordering of the Eu 4f moments [45].

Furthermore, the system displays pronounced non-Fermi liquid behavior evidenced by the linear electrical resistivity and the logarithmic divergence of S/T depicted in Fig. 5. These signatures are similar to those for optimally doped $Eu_{1-x}K_xFe_2As_2$ [17]. However, we note that a recent detailed study of the x dependence of the scattering rates in $EuFe_2(As_{1-x}P_x)_2$ determined by ARPES has found a linear energy dependence but no enhancement near the putative QCP [46]. The "strange metal" normal state properties have thus been interpreted in terms of a Lifshitz transition due to the crossing of the top (bottom) of a hole (electron) pocket through the chemical potential, causing an anomalous band dispersion at the Fermi level. The latter leads to a strong mass enhancement in the normal state.

5 Persistent magnetic detwinning 122-type iron pnictides display a strong in-plane anisotropy in various physical properties, which is much larger compared to what is expected from the orthorhombic lattice distortion. In Co-doped $BaFe_2As_2$, for example, the electrical resistivity anisotropy reaches $\rho_b/\rho_a \approx 2$, while the lattice distortion has a maximum size of $(a - b)/(a + b) = 0.36\,\%$ [47]. This observation has been associated with *electronic nematicity* and is being discussed as a relevant ingredient for high-temperature SC in these materials [6,8,48–54].

The in-plane anisotropy can only be detected by avoiding the formation of twin domains upon cooling a single crystal from the high-temperature tetragonal into the orthorhombic state. A similar problem occurs for copper oxide SCs, where magnetic and mechanical detwinning methods have been established [55, 56]. The coupling of magnetic fields of the order of several Tesla on the Fe moments is much too weak to allow a sizable detwinning [8, 57]. Instead, mechanical clamps are commonly used to apply uniaxial pressure, which in turn detwins the crystals [8]. However, this method is problematic, because the uniaxial pressure acts as an external symmetry breaking force to the system and therefore does not allow to detect the intrinsic anisotropy [52].

As mentioned above, the $EuFe_2As_2$ system is special compared to other 122 pnictides due to its magnetic Eu^{2+} moments. First evidence for a magnetically induced detwinning in this system was found by Xiao et al. while conducting neutron diffraction experiments [11]. They found a complete detwinning of $EuFe_2As_2$ in a small in-plane magnetic fields of the order of 1 T at low temperatures with the longer crystallographic a-axis parallel to the external magnetic field $H \parallel [1\,1\,0]_T$.

Recently, we have shown that this field-induced detwinning does not only work below T_N, but even persists to temperatures up to $T_s \approx 190$ K after removing the magnetic field [58]. For example, the electrical resistivity and the TEP reveal similar anisotropy as found for mechanical detwinning (see below).

In the following, we discuss these experiments, which all have been performed using a well-defined measurement protocol to ensure consistent conditions. At first, the single crystals were cooled from above T_s to low temperatures in zero magnetic field and then the "zero-field-cooled" (ZFC) response to the application of a magnetic field was detected. Here, an in-plane magnetic field was applied along the tetragonal $[1\,1\,0]_T$-direction. Afterward, the field has been removed again before conducting further measurements. This leaves the crystal aligned with the shorter b-axis parallel to the previous field direction. We call this process "field treatment" (FT).

The detwinning effect is strongly visible in the temperature-dependent resistivity $\rho(T)$ after FT. Figure 6a and b shows such data normalized to the ZFC curve. Although the magnetic field is zero during the measurement a large in-plane anisotropy along the orthorhombic axes is clearly resolved. The anisotropy changes sign, depending on FT the sample above or below T_N, but it remains almost unchanged up to T_s [58]. The thermal expansion (TE), $\Delta L(T)/L$ depicted in Fig. 6c exhibits a similar behavior as the sample is shorter after FT at 4 T than in the ZFC state, indicating a detwinning with the smaller b-axis parallel to the applied magnetic field. Remarkably, the induced imbalance (adjusted for temperature-related changes in the lattice parameters) stays virtually constant up to T_s [58].

While the electrical resistivity and the TE show only the effect of the FT, magnetostriction $\Delta L(H)/L$, and magnetoresistance $\Delta\rho(H)/\rho(H=0)$ data shown in Fig. 6d–f provide

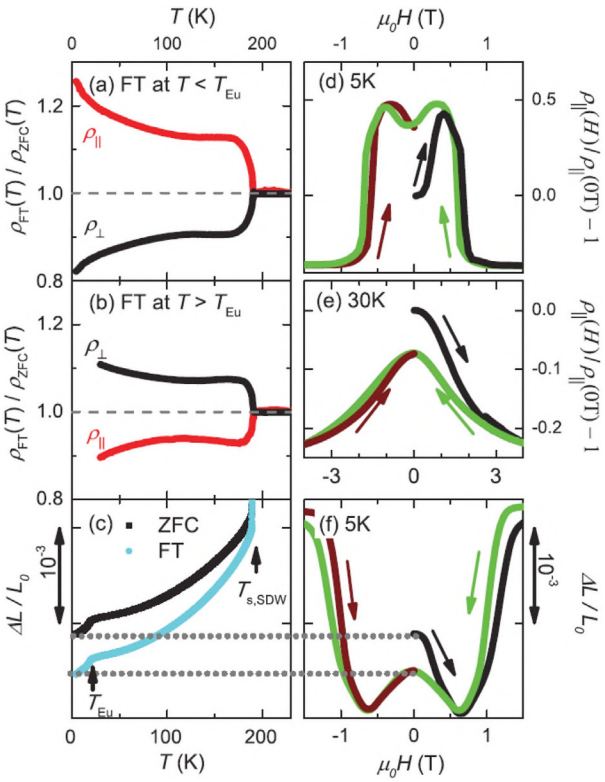

Figure 6 (Magneto)resistance, magnetostriction, and thermal expansion of ZFC $EuFe_2As_2$ with magnetic field $H \parallel [1\,1\,0]_T$. (a–b) Normalized resistivity versus temperature $\rho_{FT}(T)$ after field treatment (FT) with 4 T and current parallel (red) and perpendicular (black) to H. The FT at (a) $T = 4$ K and (b) 30 K results in opposite behavior. (c) Thermal expansion $\Delta L(T)/L_0$ ($\Delta L \parallel H$) after ZFC (black) and FT with 2 T at 4 K (cyan). (d–e) Magnetoresistance $\rho_\parallel(H)/\rho_\parallel(0\text{ T}) - 1$ at (d) 5 K and (e) 30 K. (f) Magnetostriction $\Delta L(H)/L_0$ at 5 K for increasing (black, brown) and decreasing (green) H. Replotted from Ref. [58].

insight into the detwinning process. The crystal (see Fig. 6f) initially shrinks with increasing magnetic field. Around 0.6 T, the crystal abruptly expands until the expansion saturates roughly at 2 T. After removing the magnet field, the initial length is not recovered (see Fig. 6c and f, dotted lines) and the sample remains shorter. This observation is compatible with a reorientation of the structural domains: first with the shorter b-axis parallel to the magnetic field then with the longer a-axis [58]. This behavior is also in accordance with the magnetoresistance depicted in Fig. 6d, when considering, that the shorter b-axis has a higher resistivity than the longer a-axis [8, 59]. Thus, when the sample contracts, the resistivity increases and vice versa. Therefore, we conclude that two separate detwinning processes take place during FT below T_N: an orientation of the b-axis parallel to H for low magnetic fields and a reorientation of the domains with the a-axis parallel to H at higher fields. Above T_N, however, only one, the latter detwinning process occurs, as shown in Fig. 6e for the electrical resistivity.

In the following, we present further evidence that the observed behavior is indeed related to Eu and the reorientation of structural domains. The observed magnetostriction is of the order of 10^{-3} and exceeds the typical (electronic) magnetostriction of Eu-based materials by at least two orders of magnitude. Figure 7 shows a comparison between magnetostriction data taken on $EuFe_2As_2$ with the magnetic field applied along $[1\,1\,0]_T$ (see Fig. 7a, also cf., Fig. 6f) and $[1\,0\,0]_T$ (see Fig. 7b) as well as $BaFe_2As_2$ with the field along $[1\,1\,0]_T$ (see Fig. 7c). Substituting Eu by Ba in measurements parallel to $[1\,1\,0]_T$ shows no comparable signal. The same holds when the Eu sample is rotated by 45°. At the $[1\,0\,0]_T$ direction, the easy axis of both twin types lies at an angle of 45° with respect to the magnetic field. This configuration favors no twin and thus no detwinning occurs.

From these measurements, we developed a simple model for the detwinning mechanism which is depicted in Fig. 8 [58]. It is based on the magnetocrystalline anisotropy

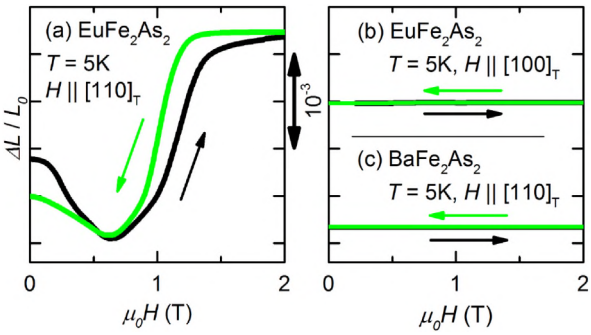

Figure 7 (a) Magnified magnetostriction of $EuFe_2As_2$ with the magnetic field $H \parallel [1\,1\,0]_T$. (b) Reference measurements of the same and a $BaFe_2As_2$ single crystal with $H \parallel [1\,0\,0]_T$ and $H \parallel [1\,1\,0]_T$ configuration, respectively. All data are plotted on the same scale and were taken at 5 K. Detwinning is only observed for $EuFe_2As_2$ with $H \parallel [1\,1\,0]_T$. Replotted from Supplement of Ref. [58].

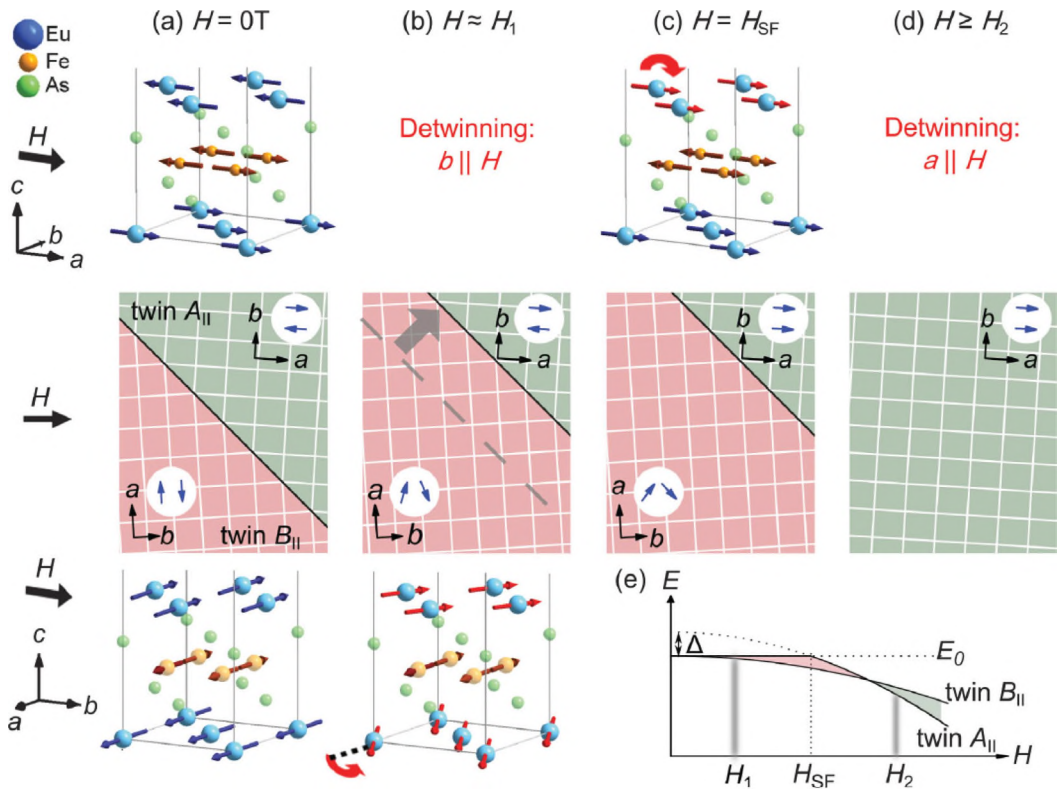

Figure 8 Depiction of the detwinning model for a (from left to right, increasing) magnetic field $H \parallel [1\,1\,0]_T$ applied at $T < T_N$. The top and bottom rows show sections of the $EuFe_2As_2$ crystal and magnetic structure [Eu atoms and spins (blue), Fe atoms (yellow) and spins (brown), and As atoms (green)] for $A_\parallel$ and $B_\parallel$ twin type configurations, respectively. Arrows indicate spin directions. The corresponding twin distribution is sketched in the middle row. (a) At $H = 0$ T, the crystal is twinned and the domains are equally distributed. The a-type AF structure leaves the Eu^{2+} moments aligned along the crystallographic a-axis. (b) Eu^{2+} moments of the $B_\parallel$ twin type (red, bottom) reduce their Zeeman energy by following the increasing magnetic field, leading to a growth of this domain type at the expense of variant $A_\parallel$ once the energy difference exceeds the twin boundary pinning energy. (c) At (higher) H_{SF} half of the Eu^{2+} moments of the remaining $A_\parallel$ type twins start lowering their energy by flipping in field direction. (d) This leads to a re-population of the $A_\parallel$ type twin once the energy is lower than the energy of the $B_\parallel$ type twin, eventually leading to a fully detwinned crystal with the a-axis parallel to H. (e) Corresponding energy curves (E_0: twinned ground state). At lower fields, the $B_\parallel$ twins are energetically favored (red area), while at higher fields the $A_\parallel$ twins are favored (green area). The detwinning takes place at H_1 and H_2, when the energy gain exceeds the pinning energies of the twin boundaries. Replotted from Ref. [58].

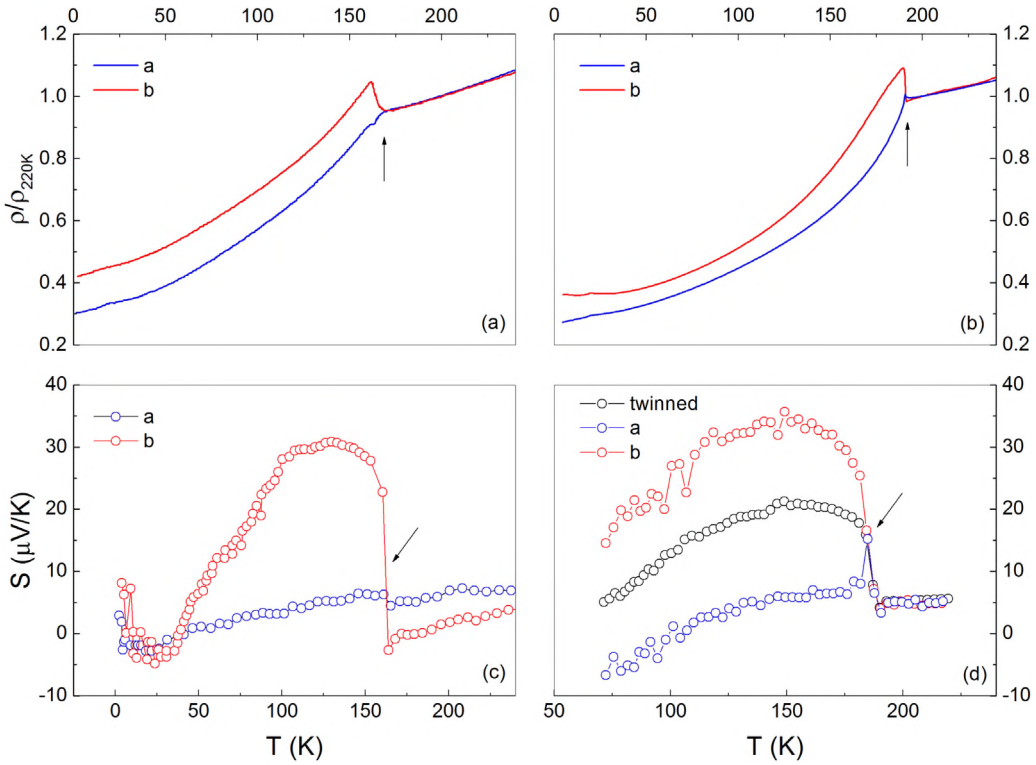

Figure 9 Electrical resistivity and thermoelectric power of (a,c) a mechanically detwinned $EuFe_2(As_{1-x}P_x)_2$ sample with $x = 0.05$ and (b,d) a magnetically detwinned $EuFe_2As_2$ crystal along their orthorhombic *a*- and *b*-axis. The in-plane anisotropy can be resolved in both cases. Arrows indicate the structural/SDW phase transitions. Data in (a,c) replotted from Ref. [53].

Δ, the AF exchange coupling J, and the Zeeman energy, but does not directly incorporate the 3d moments of the Fe sublattice.

Consider two twin types, one with the easy *a*-axis parallel to H – which we will refer to as $A_\parallel$ – and another one perpendicular – called $B_\parallel$. After ZFC, the crystal is twinned with equally distributed domains. At $T < T_N$ and $H \parallel [1\,1\,0]_T$ each domain has an energy minimum at

$$E_{min}^{B_\parallel} = E_0 - \frac{M^2(\mu_0 H)^2}{2JM^2 + \Delta}, \quad (1)$$

$$E_{min}^{A_\parallel} = E_0 + \Delta - \frac{M^2(\mu_0 H)^2}{2JM^2 - \Delta}, \quad (2)$$

with the ground state energy E_0.

At low fields (H_1), the Eu^{2+} moments of the $B_\parallel$ twin gradually rotate toward H, reducing their Zeeman energy. In the $A_\parallel$ twin, the antiparallel moments are kept in place by the magnetocrystalline anisotropy and the system keeps occupying the former ground state. The domain population shifts toward more $B_\parallel$ twins once the energy difference $E_{min}^{B_\parallel} - E_{min}^{A_\parallel}$ exceeds the pinning energies of the twin boundaries.

At $H_{SF} > H_1$, the magnetic field induces a spin flip of the antiparallel moments in the $A_\parallel$ twins. This causes $E_{min}^{A_\parallel}$ to also reduce with increasing magnetic fields, according to Eq. (2) which is plotted in Fig. 8e. The slope of $E_{min}^{A_\parallel}$ is greater than that of $E_{min}^{B_\parallel}$ due to the anisotropy – the spins of $A_\parallel$ are parallel to the systems easy axis. The two energies intersect at

$$\tilde{B} = \frac{1}{M}\sqrt{2J^2M^4 - \frac{\Delta^2}{2}}.$$

The domain population shifts toward more $A_\parallel$ twins once the energy difference $E_{min}^{A_\parallel} - E_{min}^{B_\parallel}$ again exceeds the pinning energies of the twin boundaries.

At $T > T_N$, the Eu^{2+} moments are paramagnetic and can *all* gradually align along the magnetic field. This detwins the crystal with $a \parallel H$.

In short, we have a two-step detwinning process at $T < T_N$, in which the crystal first detwins with the *b*-axis parallel to H and then with the *a*-axis parallel to H at higher fields. In the paramagnetic state of the Eu^{2+} moments, only the latter orientation occurs. The samples stay detwinned up to T_s in both cases.

The overall effect after FT is perhaps most prominently shown in Fig. 9. On the left side measurements of the electrical resistivity and the TEP performed in the typical "clamped" setup are shown, where a mechanical clamp was used to apply an uniaxial pressure of roughly 6 MPa to the sample during measurements. The anisotropy in the orthorhombic phase is visible together with an anisotropy

above T_s that has a reversed sign. This has been discussed to arise from two contributions due to anisotropic scattering and orbital polarization above and below T_s, respectively [53]. On the right side, the same set of measurements is presented. Instead of the mechanical clamp, the magnetic detwinning was used to resolve the low-temperature anisotropy. An anisotropy above T_s is not evident.

Field-induced detwinning has also been used to investigate the in-plane anisotropy of the optical conductivity, where a higher Drude weight and lower scattering rate was found along the crystallographic a-axis [58, 60].

Since Eu^{2+} has a spin-only moment, the large magnetostriction related to the field-induced detwinning must arise from an indirect coupling between the 4f moments and the lattice, via the Fe 3d moments [58]. The relevance of RKKY coupling to $EuFe_2As_2$ has been pointed out previously [41]. A preliminary study on $EuFe_2(As_{1-x}P_x)_2$ showed a weakening of the field-induced detwinning with P substitution and complete disappearance for $x = 0.14$ [61]. Nevertheless, even for samples with $x = 0.19$ which display superconductivity, ^{57}Fe Mössbauer spectroscopy has found a significant coupling between the 3d and 4f magnetic subsystems, evidenced by an enhancement of Fe spin dynamics by Eu spin fluctuations at low temperatures [62]. This coupling, however, does not lead to a bottleneck effect in the Eu spin relaxation via the conduction electrons in electron spin resonance [63].

6 Conclusions Compared to other 122 pnictides, $EuFe_2As_2$ is special due to the presence of additional 4f Eu^{2+} magnetic moments. It appears that they have only weak influence on the electronic properties. However, their indirect coupling to the lattice via the Fe moments allows to use magnetic fields to very effectively detwin single crystals. Quite remarkably, fields of only 1 T induced a persistent (even after field is reduced to zero) detwinning which holds upon warming up to the structural phase transition of almost 200 K. Related to the field-induced detwinning, a very large (for Eu magnets) isothermal magnetostriction has been found. Our studies of the electrical resistivity and TEP prove that field-induced detwinning allows to investigate the in-plane anisotropy in $EuFe_2As_2$.

We have also reviewed the structural and magnetic properties of the hole-doped $Eu_{1-x}K_xFe_2As_2$ and chemically pressurized $EuFe_2(As_{1-x}P_x)_2$ alterations. These systems exhibit rich phase diagrams with indications for non-Fermi liquid behavior, evident from the T-linear resistivity and the diverging temperature behavior of the TEP divided by temperature. These effects could be related to Lifshitz transitions that trigger the breaking of Fermi surface nesting and leads to a suppression of Fe magnetic ordering and the occurrence of superconductivity. For $EuFe_2(As_{1-x}P_x)_2$ a very narrow SC dome has been found with coexistence of FM Eu ordering.

Acknowledgements We thank N. Bach, U. Bovensiepen, M. Dressel, J. Fink, V. A. Gasparov, T. Goltz, H. S. Jeevan, S. Jiang, D. Kasinathan, H.-H. Klauss, S. Nandi, H.-A. Krug von Nidda, I.-M. Pietsch, H. Rosner, C. Stingl, S. Thirupathaiah, Y. Tokiwa, D. Wu, Y. Xiao, and S. Zapf for collaboration on the results reviewed in this paper. Financial support by the DFG through SPP 1458 and the Alexander von Humboldt foundation is gratefully acknowledged.

References

[1] Y. Kamihara, T. Watanabe, M. Hirano, and H. Hosono, J. Am. Chem. Soc. **130**, 3296–3297 (2008).
[2] D. C. Johnston, Adv. Phys. **59**, 803–1061 (2010).
[3] I. I. Mazin, Nature **464**, 183–186 (2010).
[4] J. Paglione and R. L. Greene, Nature Phys. **6**, 645–658 (2010).
[5] P. Dai, J. Hu, and E. Dagotto, Nature Phys. **8**, 709–718 (2012).
[6] R. Fernandes, A. Chubukov, and J. Schmalian, Nature Phys. **10**, 97–104 (2014).
[7] M. Rotter, M. Tegel, D. Johrendt, I. Schellenberg, W. Hermes, and R. Pöttgen, Phys. Rev. B **78**, 020503 (2008).
[8] I. R. Fisher, L. Degiorgi, and Z. X. Shen, Rep. Prog. Phys. **74**, 124506 (2011).
[9] S. Jiang, Y. Luo, Z. Zhu, C. Wang, X. Xu, Q. Tao, G. Cao, and Z. Xu, New J. Phys. **11**, 025007 (2009).
[10] Y. Xiao, Y. Su, M. Meven, R. Mittal, C. M. N. Kumar, T. Chatterji, S. Price, J. Persson, N. Kumar, S. K. Dhar, A. Thamizhavel, and T. Brueckel, Phys. Rev. B **80**, 174424 (2009).
[11] Y. Xiao, Y. Su, W. Schmidt, K. Schmalzl, C. M. N. Kumar, S. Price, T. Chatterji, R. Mittal, L. J. Chang, S. Nandi, N. Kumar, S. K. Dhar, A. Thamizhavel, and T. Brueckel, Phys. Rev. B **81**, 220406 (2010).
[12] H. S. Jeevan, Z. Hossain, D. Kasinathan, H. Rosner, C. Geibel, and P. Gegenwart, Phys. Rev. B **78**, 052502 (2008).
[13] Z. Ren, Z. Zhu, S. Jiang, X. Xu, Q. Tao, C. Wang, C. Feng, G. Cao, and Z. Xu, Phys. Rev. B **78**, 052501 (2008).
[14] D. Wu, N. Barišić, N. Drichko, S. Kaiser, A. Faridian, M. Dressel, S. Jiang, Z. Ren, L. Li, G. Cao Z. A. Xu, H. S. Jeevan, and P. Gegenwart, Phys. Rev. B **79**, 155103 (2009).
[15] S. Jiang, H. Xing, G. Xuan, Z. Ren, C. Wang, Z. A. Xu, and G. Cao, Phys. Rev. B **80**, 184514 (2009).
[16] H. S. Jeevan, Z. Hossain, D. Kasinathan, H. Rosner, C. Geibel, and P. Gegenwart, Phys. Rev. B **78**, 092406 (2008).
[17] J. Maiwald, H. S. Jeevan, and P. Gegenwart, Phys. Rev. B **85**, 024511 (2012).
[18] C. F. Miclea, M. Nicklas, H. S. Jeevan, D. Kasinathan, Z. Hossain, H. Rosner, P. Gegenwart, C. Geibel, and F. Steglich, Phys. Rev. B **79**, 212509 (2009).
[19] T. Terashima, M. Kimata, H. Satsukawa, A. Harada, K. Hazama, S. Uji, H. Suzuki, T. Matsumoto, and K. Murata, J. Phys. Soc. Jpn. **78**, 083701 (2009).
[20] H. S. Jeevan and P. Gegenwart, J. Phys. Conf. Ser. **200**, 012060 (2010).
[21] S. de Jong, E. van Heumen, S. Thirupathaiah, R. Huisman, F. Massee, J. Goedkoop, R. Ovsyannikov, J. Fink, H. Dürr, A. Gloskovskii, H. S. Jeevan, P. Gegenwart, A. Erb, L. Patthey, M. Shi, R. Follath, A. Varykhalov, and M. S. Golden, Europhys. Lett. **89**, 27007 (2010).
[22] S. Thirupathaiah, E. Rienks, H. S. Jeevan, R. Ovsyannikov, E. Slooten, J. Kaas, E. van Heumen, S. de Jong, H. Dürr, K. Siemensmeyer, R. Follath, P. Gegenwart, M. S. Golden, and J. Fink, Phys. Rev. B **84**, 014531 (2011).
[23] L. Rettig, R. Cortés, S. Thirupathaiah, P. Gegenwart, H. S. Jeevan, M. Wolf, J. Fink, and U. Bovensiepen, Phys. Rev. Lett. **108**, 097002 (2012).

[24] I. Avigo, R. Cortés, L. Rettig, S. Thirupathaiah, H. S. Jeevan, P. Gegenwart, T. Wolf, M. Ligges, M. Wolf, J. Fink, and U. Bovensiepen, J. Phys.: Condens. Matter **25**, 094003 (2013).

[25] D. Wu, G. Chanda, H. S. Jeevan, P. Gegenwart, and M. Dressel, Phys. Rev. B **83**, 100503 (2011).

[26] N. Pascher, J. Deisenhofer, H. A. K. von Nidda, M. Hemmida, H. S. Jeevan, P. Gegenwart, and A. Loidl, Phys. Rev. B **82**, 054525 (2010).

[27] V. A. Gasparov, A. Audouard, L. Drigo, A. I. Rodigin, C. T. Lin, W. P. Liu, M. Zhang, A. F. Wang, X. H. Chen, H. S. Jeevan, J. Maiwald, and P. Gegenwart, Phys. Rev. B **87**, 094508 (2013).

[28] V. Gasparov, H. S. Jeevan, and P. Gegenwart, J. Exp. Theor. Phys. **89**, 294–297 (2009).

[29] K. Kihou, T. Saito, S. Ishida, M. Nakajima, Y. Tomioka, H. Fukazawa, Y. Kohori, T. Ito, S. ichi Uchida, A. Iyo, C. H. Lee, and H. Eisaki, J. Phys. Soc. Jpn. **79**, 124713 (2010).

[30] M. Gooch, B. Lv, B. Lorenz, A. M. Guloy, and C. W. Chu, Phys. Rev. B **79**, 104504 (2009).

[31] I. Paul and G. Kotliar, Phys. Rev. B **64**, 184414 (2001).

[32] Y. Tokiwa, S. H. Hübner, O. Beck, H. S. Jeevan, and P. Gegenwart, Phys. Rev. B **86**, 220505 (2012).

[33] H. S. Jeevan, D. Kasinathan, H. Rosner, and P. Gegenwart, Phys. Rev. B **83**, 054511 (2011).

[34] S. Kasahara, T. Shibauchi, K. Hashimoto, K. Ikada, S. Tonegawa, R. Okazaki, H. Shishido, H. Ikeda, H. Takeya, K. Hirata, T. Terashima, and Y. Matsuda, Phys. Rev. B **81**, 184519 (2010).

[35] Y. Nakai, T. Iye, S. Kitagawa, K. Ishida, H. Ikeda, S. Kasahara, H. Shishido, T. Shibauchi, Y. Matsuda, and T. Terashima, Phys. Rev. Lett. **105**, 107003 (2010).

[36] Z. Ren, Q. Tao, S. Jiang, C. Feng, C. Wang, J. Dai, G. Cao, and Z. Xu, Phys. Rev. Lett. **102**, 137002 (2009).

[37] One possibility for the discrepancy between our results on single crystals with that on polycrystals [36] could be an inhomogeneous contribution of the P content in the latter.

[38] S. Nandi, W. Jin, Y. Xiao, Y. Su, S. Price, W. Schmidt, K. Schmalzl, T. Chatterji, H. S. Jeevan, P. Gegenwart, and T. Brückel, Phys. Rev. B **90**, 094407 (2014).

[39] S. Zapf, D. Wu, L. Bogani, H. S. Jeevan, P. Gegenwart, and M. Dressel, Phys. Rev. B **84**, 140503 (2011).

[40] S. Thirupathaiah, E. D. L. Rienks, H. S. Jeevan, R. Ovsyannikov, E. Slooten, J. Kaas, E. van Heumen, S. de Jong, H. A. Dürr, K. Siemensmeyer, R. Follath, P. Gegenwart, M. S. Golden, and J. Fink, Phys. Rev. B **84**, 014531 (2011).

[41] A. Akbari, I. Eremin, and P. Thalmeier, Phys. Rev. B **84**, 134513 (2011).

[42] A. A. Abrikosov and L. P. Gor'kov, J. Exp. Theor. Phys. **12**, 1243 (1961).

[43] S. Nandi, W. Jin, Y. Xiao, Y. Su, S. Price, D. Shukla, J. Strempfer, H. Jeevan, P. Gegenwart, and T. Brückel, Phys. Rev. B **89**, 014512 (2014).

[44] N. Kurita, K. Kodama, A. Harada, M. Tomita, H. S. Suzuki, T. Matsumoto, K. Murata, S. Uji, and T. Terashima, Phys. Rev. B **88**, 224510 (2013).

[45] S. Zapf, H. S. Jeevan, T. Ivek, F. Pfister, F. Klingert, S. Jiang, D. Wu, P. Gegenwart, R. K. Kremer, and M. Dressel, Phys. Rev. Lett. **110**, 237002 (2013).

[46] J. Fink, A. Charnukha, E. Rienks, Z. Liu, S. Thirupathaiah, I. Avigo, F. Roth, H. S. Jeevan, P. Gegenwart, M. Roslova, I. Morozov, S. Wurmehl, U. Bovensiepen, S. Borisenko, M. Vojta, and B. Büchner, Phys. Rev. B **92**, 201106 (2015).

[47] J. H. Chu, J. G. Analytis, K. De Greve, P. L. McMahon, Z. Islam, Y. Yamamoto, and I. R. Fisher, Science **329**, 824–826 (2010).

[48] M. A. Tanatar, E. C. Blomberg, A. Kreyssig, M. G. Kim, N. Ni, A. Thaler, S. L. Bud'ko, P. C. Canfield, A. I. Goldman, I. I. Mazin, and R. Prozorov, Phys. Rev. B **81**, 184508 (2010).

[49] M. Yi, D. Lu, J. H. Chu, J. G. Analytis, A. P. Sorini, A. F. Kemper, B. Moritz, S. K. Mo, R. G. Moore, M. Hashimoto, W. S. Lee, Z. Hussain, T. P. Devereaux, I. R. Fisher, and Z. X. Shen, Proc. Natl. Acad. Sci. USA **108**, 6878–6883 (2011).

[50] S. Kasahara, H. Shi, K. Hashimoto, S. Tonegawa, Y. Mizukami, T. Shibauchi, K. Sugimoto, T. Fukuda, T. Terashima, A. H. Nevidomskyy, and Y. Matsuda, Nature **486**, 382–385 (2012).

[51] J. H. Chu, H. H. Kuo, J. G. Analytis, and I. R. Fisher, Science **337**, 710–712 (2012).

[52] C. Dhital, Z. Yamani, W. Tian, J. Zeretsky, A. S. Sefat, Z. Wang, R. J. Birgeneau, and S. D. Wilson, Phys. Rev. Lett. **108**, 087001 (2012).

[53] S. Jiang, H. S. Jeevan, J. Dong, and P. Gegenwart, Phys. Rev. Lett. **110**, 067001 (2013).

[54] E. P. Rosenthal, E. F. Andrade, C. J. Arguello, R. M. Fernandes, L. Y. Xing, X. C. Wang, C. Q. Jin, A. J. Millis, and A. N. Pasupathy, Nature Phys. **10**, 225–232 (2014).

[55] A. N. Lavrov, Y. Ando, S. Komiya, and I. Tsukada, Phys. Rev. Lett. **87**, 017007 (2001).

[56] A. Lavrov, S. Komiya, and Y. Ando, Nature **418**, 385–386 (2002).

[57] J. H. Chu, J. G. Analytis, D. Press, K. De Greve, T. D. Ladd, Y. Yamamoto, and I. R. Fisher, Phys. Rev. B **81**, 214502 (2010).

[58] S. Zapf, C. Stingl, K. Post, J. Maiwald, N. Bach, I. Pietsch, D. Neubauer, A. Löhle, C. Clauss, S. Jiang, H. S. Jeevan, D. N. Basov, P. Gegenwart, and M. Dressel, Phys. Rev. Lett. **113**, 227001 (2014).

[59] E. Blomberg, M. Tanatar, R. Fernandes, I. Mazin, B. Shen, H. H. Wen, M. Johannes, J. Schmalian, and R. Prozorov, Nature Commun. **4**, 1914 (2013).

[60] S. Zapf, D. Neubauer, K. W. Post, A. Kadau, J. Merz, C. Clauss, A. Löhle, H. S. Jeevan, P. Gegenwart, D. N. Basov, and M. Dressel, C.R. Phys. **17**, 188–196 (2016).

[61] I. Pietsch, Thermal Expansion and Magnetostriction Measurements of $EuFe_2(As_{1-x}P_x)_2$, Master's thesis, University of Göttingen (2014).

[62] T. Goltz, S. Kamusella, H. S. Jeevan, P. Gegenwart, H. Luetkens, P. Materne, J. Spehling, R. Sarkar, and H. H. Klauss, J. Phys. Conf. Ser. **551**, 012025 (2014).

[63] H. A. K. von Nidda, S. Kraus, S. Schaile, E. Dengler, N. Pascher, M. Hemmida, M. Eom, J. Kim, H. S. Jeevan, P. Gegenwart, J. Deisenhofer, and A. Loidl, Phys. Rev. B **86**, 094411 (2012).